Synthesis and Optimization of GO/PMMA/n-Octadecane Phase Change Nanocapsules Using Response Surface Methodology

Chananipoor, Arman; Azizi, Zoha*+; Raei, Behrouz, Tahmasebi, Nargess

Department of Chemical Engineering, Mahshahr Branch, Islamic Azad University, Mahshahr, I.R. IRAN

ABSTRACT: *Nano Encapsulated Phase Change Materials (NEPCMs) are a crucial part of solar energy systems due to their high thermal storage density. The particle size of the NEPCMs is especially of great importance due to its effect on heat transfer and long-term use during applications. In this study, nanocapsules containing Phase Change Material (PCM) n-dodecanol as core and polymethyl methacrylate (PMMA) as shell were synthesized by miniemulsion polymerization with Graphene Oxide (GO) nanosheets as an extra protective screen situated at the interface between the core and the shell. The experiments were designed with the Central Composite Design (CCD) of Response Surface Methodology (RSM). The nanocapsules synthesis experiments were conducted as per the statistical design to determine the optimum process conditions. The effect of initiator/Methyl methacrylate(MMA) mass ratio (BPO/MMA wt.%), n-octadecane/MMA mass ratio (PCM/MMA), stabilizer/MMA mass ratio (triton X-100/MMA wt.%), water/MMA mass ratio (H_2O/MMA) and GO/MMA ratio on the nanocapsule properties were investigated. The correlation between nanocapsule properties (melting latent heat and average particle size of nanocapsules) and affecting factors were evaluated and verified. The numerical optimization showed that the optimum nanoparticle size (110 nm) and latent heat (148.5 J/kg) can be obtained at H_2O/MMA of 11.3 wt%, PCM/MMA mass ratio of 1.88wt%, X-100/MMA of 10.81wt.%, and BPO/MMA of 2.96 wt.% and GO/MMAof 3.79wt%. The optimized nanocapsules were characterized by Fourier Transform InfraRed (FT-IR) spectroscopy, Transmission Electron Microscope (TEM), Differential Scanning Calorimetry (DSC), ThermoGravimetric Analysis (TGA), and laser particle diameter analyzer. The thermal cycling tests indicate the high thermal resistance of the prepared core-shell system, even after 100 heating/cooling cycles, and have an excellent potential for energy storage and release performance of the system.*

KEYWORDS: *Nanocapsules; Miniemulsion; Response surface method; Phase change; Optimization.*

INTRODUCTION

With the rapid development of society and the economy, demand for energy is increasing at an exponential rate. Due to the depletion of conventional energy sources and a series of environmental problems caused by extensive use of fossil fuels, sustainable management of energy, such as the development of new energy sources and improvement

* *To whom correspondence should be addressed.*
+ E-mail: azizi.zoha@gmail.com
1021-9986/2021/2/383-394 12/$/6.02

in utilization of existing energy sources becomes increasingly important [1-4]. Since the first oil crisis in 1970, scientists around the world have begun seeking new sources of energy and exploring new ways to manage energy. Energy storage in industrial energy conservation and new energy applications have gained the most attention; among these, low-cost phase change materials (PCMs) became popular because of their high storage capacity and thermostatic effect during energy storage [1]. PCM can absorb or release heat, change its physical state (e.g. from solid to liquid and vice versa) and provide the latent heat with changes in temperature. As the PCM undergoes physical state changes, the temperature of the material remains almost unchanged [5,6]. The use of PCM can improve the utilization of existing energy sources. PCM has been widely used in air-conditioning, building materials, textiles, energy-saving equipment, health care, food preservation and warm supplies as one of the typical environmentally friendly energy-saving materials [7].

PCMs are divided into three main categories, namely organic, inorganic and eutectics [8]. Paraffins and n-alkanes, as organic substances are of prodigious attention, due to their high latent heat, chemical and thermal stability, low vapor pressure, cheapness and accessibility [9]. Encapsulation has resolved the shortcomings of PCMs. PCM nanocapsules are made up of nano-materials in a shell that coats the surface of another material [10]. The nanocapsules technology helps eliminate the problem of material leakage when the PCM is melted, and provides a large heat transfer area because of the small particle size and large surface area of the encapsulated material [11]. Nanometer sized NanoPCMs have much larger specific surface area than macro or micro encapsulated PCMs, which can result in much faster thermal energy storage/release. In addition, when applied in Latent Functionally Thermal Fluid (LFTF), NanoPCMs do not fracture easily in the course of flow[12]. Therefore, NanoPCMs have attracted much interest and significant development has been achieved [8]. *Sarı et al.* [13] and *Chen et al.* [14] synthesized nanocapsules with PMMA as a shell containing n-octacosane and n-dodecanol as the core, respectively, by miniemulsion polymerization method. *Zhang et al.* [15] and *Tumirah et al.* [16] synthesized nanocapsules containing n-OD as the core, with poly(ethyl methacrylate), PMMA, and poly(styrene-co-methyl methacrylate) shells, respectively. *Fang et al.* [17] reported PS nanoencapsulated n-tetradecane for cold thermal energy storage. *Latibari et al.* [18] focused on NanoPCMs containing fatty acids (palmitic acid, stearic acid) as core and inorganic materials (SiO_2, TiO) as shell for thermal energy storage applications. *Zhu* [19, 20] reported nanocapsules containing n-OD as core with organosilica shells achieved by facile interfacial hydrolysis-condensation reaction in miniemulsion, and studied the morphological control and thermal properties of these NanoPCMs.

However, most of the PCM nanocapsules with low thermal conductivities which are highly undesirable in heat transfer application [21]. The nanoencapsulation materials are mostly made up of organic polymer, contributing to the very low thermal conductivities. Although the encapsulation materials can prevent leakage of PCMs, they slow down the rate of heat transfer, resulting in a reduction in PCM energy storage or cooling effect [22]. Adding materials with higher thermal conductivity is a method that can be employed to increase the rate of heat transfer [2, 8, 23-25].

Graphene and its derivatives have gained significant attention and have become one of the most widely investigated materials as their superior properties. Graphene Oxide (GO), one of the derivatives of graphene, has many advantages of light weight, large surface areas, and low thickness (the monolayer thickness of GO is about 1–1.4 nm)[26]. And as reported in literature, the elastic modulus of GO is 207.6 ± 23.4 GPa, which is high enough for being used as a reinforcing material to compensate for the defects of polymer shells. Moreover, recent studies have demonstrated that GO can be used for enhancing thermal properties [27]. So GO is a kind of suitable material to improve the leakage-prevention and thermal performance. In addition, GO consists of myriad oxygen functional groups such as hydroxyl, carbonyl, epoxy and carboxylic groups [28], and these hydrophilic functional groups on the hydrophobic carbon layers endow GO with amphiphilicity, which promotes GO to be assembled at the oil-water interface. Therefore, GO can be used to stabilize emulsions [29]. *Zhang et al.* [26] reported novel microencapsulated phase change materials (MEPCMs) with a high encapsulation capacity and enhanced leakage-prevention performance by in situ polymerization. For MEPCMs, paraffin and melamine-formaldehyde resin (MF) were respectively used as core and shell, and

Graphene Oxide (GO) nanosheets were situated at the interface between the core and the shell.

To fabricate the nanocapsules containing PCM materials, nanoemulsion should be formed firstly, followed by the construction of the shell on the surface of nanoemulsion droplets. Zhang et al. synthesized micro- and nanocapsules containing PCM n-octadecane as core material and melamine-formaldehyde (MF) as shell material by in-situ polymerization [16]. The emulsion was prepared with a homomixer at stirring rates of 3000–9000 rpm, then the MF prepolymer was added into the emulsion and stirred at a rate of 600 rpm to form micro- and nanocapsules. Fan et al. fabricated nanocapsule containing n-octadecane (91.2%) and cyclohexane (8.8%) as core material and MF as the shell material through in-situ polymerization [13]. Both teams used the homogenizer to produce nanoemulsion. Compared with homogenization treatment with a homogenizer, the ultrasound-assisted production of nanoemulsion has gained more attention because of the reverse piezoelectric effect, high energy efficiency, low production cost, and simple system operation [14-16, 17, 18]. *Zhu et al.* [20] successfully prepared micro- and nanocapsules containing n-dodecane with MF resin as the shell material by in-situ polymerization. For preparing microcapsules, the emulsion was formed after the homogenization treatment for 10 min with a homogenizer at a given rate in the range of 2400–18,000 rpm.

Although many studies have been performed in fabricating and characterizing of NPCMs, the studies on the nanocapsules with GO sheets are sure to be of higher interest for their lower leakage rate and higher heat transfer speed. To the best of our knowledge, there is no comprehensive study to investigate NPCMs both leakage and thermal performance simultaneously. In addition, polystyrene with high hydrophobicity is the most applied polymer shell material in nanoencapsulation process. However, few reports considered the nano-encapsulation via miniemulsion polymerization with lower hydrophilicity shell material like polymethyl methacrylate (PMMA). In addition, impact of different factors has not been fully addressed during the nanocapsules fabricating. The aim of this study was to synthesize PCMs nanocapsules with graphene/PMMA hybrid structure shells. The morphologies and microstructure of nanocapsules had been systemically analyzed. The relationship of the nanostructure changes and thermal performances of the nanocapsules with their components has been investigated using response surface method.

EXPERIMENTAL SECTION

Methyl methacrylate(MMA) (99 wt%, SigmaeAldrich, Co., Germany) was utilized as the monomer for the formation of shell. Triton X-100 (SigmaeAldrich Co., USA) was employed as stabilizer agent, BPO (Polyvinyl alcohol, SigmaeAldrich, Co., USA) was used as oil soluble initiator. The n-Octadecane (Aramis, Co., USA) was used as organic core (PCM). GO (graphen oxide, Sigmae Aldrich, Co., USA) was used as a reducing leakage agent and also as a promoting of the shell thermal conductivity. Nitrogen gas was of high-puritygrade.

Preparation of NEPCMs

Miniemulsion polymerization was used to synthesize the nanocapsules. Triton X-100, GO and deionized water were mixed together (solution A) according to the ratio listed in the RSM design table. Ultrasonic cell disruptor was used to obtain the stable aqueous phase for 30 min in ice-water bath. The MMA, PCM and BPO were mixed together as the oil phase. The pre-emulsion was obtained by adding oil phase into the solution A and mixing mechanically at the stirring rate of 1500 rpm for 30 min. The pre-emulsion was dispersed around 10 min in ultrasonic cell to obtain miniemulsion. Four-necked flask equipped with a mechanical stirrer was employed in NPCM fabricating process. The flask consists of nitrogen inlet and reflux condenser. The miniemulsion was placed into the flask and then was heated to start a miniemulsion polymerization under the stirring. The reaction temperature and stirring rate were set to 95 ˚C and 1700rpm, respectively. After 6 h, the nanocapsule latex containing PCM was appeared which slowly cooled down to room temperature. The resultant nanocapsule latex was demulsified by adding the mixture of ethanol and 50 wt.% aqueous sodium chloride solution, and then the demulsified latex was filtered to obtain the solid sample of nanocapsule containing PCM. Finally, the solid nanocapsule was washed with 50 wt.% ethanol-water solution of 50 °C for once and with distilled water for twice to remove the unencapsulated n-Octadecane, and then was left out to dry at 30 °C for 24 h under vacuum.

Experimental design and mathematical modeling

Design of experiments and Response surface methodology (RSM) were used to evaluate the effects of different variables on ceiling fan performance. The RSM shows not only the optimum conditions, but also proposes fitted regression models. The CCD (central composite design) under RSM was used to characterize the interaction between the process variables and the response. Preliminary experiments were performed for determination of the independent variables and their experimental ranges to design the experimental runs. Based on the literature and the preliminary results, the most important operating variables, which affect the nanocapsule size and latent heat are the ratios of H_2O/MMA (A), X-100/MMA (B), PCM/MMA (C), BPO/MMA (D) and GO/MMA (E). These parameters were considered as the system independent variables and nanocapsules properties like size and the values of latent heat were considered as the process responses. Table 1 shows experimental design based on CCD used in this study.

A set of 32 experimental runs, including duplicates was designed using the CCD. All statistical analyses were carried out using Design Expert V.11. The adequacy of the predictive models was assessed using a lack of fit F-test by comparing the modeling error (lack of fit) with the experimental error (pure error) calculated from the replicates of center points in the CCD, which allows determination of whether the modeling error is significantly different from the pure error. If the lack of fit test is statistically significant, the adequacy of the model will be further verified by checking other summary statistics such as predicted R^2, adequate precision, and predicted error sum of squares (PRESS). The coefficients for the response surface models were estimated using multiple regression analysis, and their significance tested by a t-test. A ridge analysis was carried out to determine the region, for which the lowest/highest factors were expected. The comparison of response between those predicted by model and those measured by simulation was conducted using Student's t-tests, while all responses in the central points were pooled after conducting Levene's test for homogeneity of variances, and then compared using a Student's t-test''. After performing sensitivity analysis, the process was optimized.

Characterization of nanocapsules

Nicolet 6700 IR spectrophotometer was used to obtain the FT-IR spectra. The surface morphology of the NPCM were studied using a 30 PhilipS XL FESEM and Hitachi H-800TEM. Based on FESEM image, NPCM particlesize distribution (PSD) was conducted by using Nano Measurer 1.2 software. Thermal stability of encapsulated PCM with melting/solidifying cycles was measured with Binder MK240 high-low temperature chamber which operates between 5 °C and 40 °C. leakage rate (Lr) was measured in an oven to investigate the leakage-prevention performance of the sample. A specific amount of the sample (M_0=1.0 g, M_0 is the initial mass) were placed on the filter papers separately and then transferred into the oven (at 60 °C). The samples were further removed regularly from the oven in order to measure their weight and replace the filter papers. The mass of the samples after being heated in the oven during each time span was labeled as (M_n) . The leakage rate is calculated by Eq. (1):

$$Lr(\%) = \frac{M_0 - M_n}{M_0} \times 100 \quad (1)$$

RESULTS AND DISCUSSION

A 5 factor 5 level CCD RSM was performed to investigate the relation between the combined effects of individual factors to the responses. To minimize systematic error, the experiments were carried out randomly [30]. No transformation was chosen while analyzing the response. Data from CCD were expressed by second-order polynomial model. The regression equations with coded variables obtained according to Eqs. (2) and (3):

$$d_{NEPCM} = 387.02 - 4.286A + 18.423B - 318.62C + 97.37D - 37.28E - 1.717AB + 21.617AC - 11.416AD + 2.47AE + 4.411BC - 8.611BD - 0.375BE + 22.352CD + 18.529CE + 3.733DE \quad (2)$$

$$H_{NEPCM} = -99.61 - 12.99A + 1.3B + 236.1C + 40.36D + 12.28E + 1.09AB - 7.38AC - 3.88AD - 1.02AE - 3.31BC + 1.74BD - 0.59BE - 5.09CD - 10CE + 0.0.52DE + 2.01A^2 - 0.30B^2 - 38.83C^2 - 6.80D_2 - 0.059E^2 \quad (3)$$

Where:

A : H_2O / MMA

B : X – 100 / MMA

C : PCM / MMA

D : BPO / MMA

E : GO / MMA

Table 1: The level of variables in CCD.

Name	Units	-1 Level	+1 Level	-α	+α
H2O/MMA1	wt/wt	4	8	2	10
X-100/MMA	wt%	6	12	3	15
PCM/MMA	wt/wt	0.65	1.5	0.225	1.925
BPO/MMA	wt%	1.75	3.25	1	4
GO/MMA	wt%	2	6	0	8

The positive sign of the coefficients in the regression equation indicated a synergistic effect, while the negative sign represented an antagonistic effect on the response.

Statistical analysis

A statistical analysis of variance (ANOVA) based on the CCD was performed to determine the fitness and the significance of the models, while also determines the effects of the individual variables and the interactions between them on the responses. The model and model terms are considered to be significant only when the values of P-Valueis less than 0.1. The ANOVA assessed the significance of the fitting of the quadratic model for the response with results shown in Tables 2 and 3.

A F-value of 8.24 with (Prob > F) for response 1 (latent heat) verified the sufficiency of the model as shown in Table 2. From the ANOVA table, the model term A and C were observed to be statistically significant. However, the model terms B, D and E were statistically insignificant. The interaction between A-H_2O/MMA and B-X-100/MMA ratios as well as the combined effect of A and C, i.e. AC, had a significant effect on the latent heat of nanocapsules. The Lack of Fit F-value of 0.73 is significant, and there is only a 27% chance that such a large Lack of Fit F-value could occur due to noise. An immaterial lack of fit is desired. The R^2 of the model for response 1 was noted as 0.86 suggesting that the polynomial equations envelop the model in a satisfactory manner. The "pred R-squared" of 0.78 was in agreement with the "adj Rsquared" of 0.79 because the difference between these values is within 0.01 confirming good predictability of the model. Moreover, the standard deviation of the model was 2.25and it has been confirmed that the predicted value obtained will be found closer to the actual value for the response (1). "Adequate precision" is a measure of the signal to noise ratio and a value not less than 4 is always desirable. In the present analysis, a value of 13.38 indicated sufficient discrimination of the model. On the other hand, a relatively lower value of the coefficient of variation (CV = 2.05%) indicated good precision and reliability of the experiments.

Results of ANOVA in Table 3 (response 2: nanocapsule size) showed that the model was highly significant according to the Fisher F-test with a very low probability value [(P > F) = 0.0001]. The main effects A, B, E and the two-level interactions of AB, AC and BE were the significant model terms (P-Value<0.05). Other model terms were statistically insignificant. Also, a high value of R^2, ca. 0.93, indicated a well predicted response values by the correlation(3) . Additionally, the adjusted R^2 value (0.89) was also high enough to suggest the significance of the model, which ensured a satisfactory fit between the polynomial model and the experimental data. Simultaneously, a low value of the coefficient of variation (CV = 2.65%) denoted good accuracy and reliability of the experiments.

The plots of the predicted versus actual results for responses 1 and 2 are shown in Fig. 1. The experimentally obtained data for each run is the actual value, whereas the predicted value is evaluated from the model using the prediction equation (3). From the plots, it was observed that most of the data points were well distributed near to the straight line, indicating an excellent relationship between the experimental and predicted values of the responses. Thus, all these statistical tests showed that the developed quadratic models are proper correlations between the process variables and the responses.

To investigate the distribution of the responses 1 and 2 graphically the Normal Probability Plots are shown in Fig. 2. Here, the data are plotted against a theoretical normal distribution and observed to be close to the straight line. This, indicates that the normal distribution is a good model for this data set.

Table 2: The results of ANOVA analysis of the developed model for NPCM latent Heat.

Response2:NCPCM Latent Heat				
ANOVA for Response Surface Quadratic Model				
Source	Mean Square	F Value	p-value Prob > F	
Model				significant
A-H_2O/MMA	44.28	0.28	0.0609	
B-X-100/MMA	114.41	0.71	0.4159	
C-PCM/MMA	18503.71	115.6	< 0.0001	
D-BPO/MMA	289.81	1.81	0.2055	
E-GO/MMA	214.8	1.34	0.2712	
AB	686.44	4.29	0.0627	
AC	630.01	3.94	0.0728	
AD	542.89	3.39	0.1926	
AE	267.32	1.67	0.2227	
BC	285.61	1.78	0.2086	
BD	246.49	1.54	0.2404	
BE	205.92	1.29	0.2808	
CD	42.25	0.26	0.6176	
CE	0.12	7.65E-04	0.9784	
DE	9.92	0.062	0.808	
A^2	1911.62	11.94	0.0054	
B^2	224.22	1.4	0.2615	
C^2	1443.41	9.02	0.012	
D^2	429.68	2.68	0.1296	
E^2	1.69	0.011	0.9201	
Residual	160.06			
Lack of Fit	274.85	12.31	0. 73	Not significant
Pure Error	22.32			

Table 3: The results of ANOVA analysis of the developed model for NPCM size.

Response1:NCPCM Size				
ANOVA for Response Surface 2FI Model				
Source	Mean Square	F Value	p-value, Prob > F	
Model	4908.23	6.61	0.0003	significant
A-H_2O/MMA	22082.67	29.75	< 0.0001	
B-X-100/MMA	22326	30.08	< 0.0001	
C-PCM/MMA	1600.67	2.16	0.1014	
D-BPO/MMA	1261.5	1.7	0.2108	
E-GO/MMA	1120.67	1.51	0.0237	
AB	1699.09	2.29	0.0498	
AC	5402.25	7.28	0.0158	
AD	4692.25	6.32	0.1232	
AE	1561.83	2.1	0.1662	
BC	506.25	0.68	0.4211	
BD	6006.25	8.09	0.1117	
BE	81	0.11	0.0344	
CD	812.25	1.09	0.3111	
CE	3969	5.35	0.7454	
DE	501.76	0.68	0.4231	
Residual	742.33			
Lack of Fit	1064.07	30.83	0.70	Not significant
Pure Error	34.51			

Fig.3 shows Perturbation plots for both responses. For response surface designs, the perturbation plot shows how the response changes as each factor moves from the chosen reference point, with all other factors held constant at the reference value. As stated before and Fig. 3(a) reveals that factors B, D and E has a relatively small effect on LH as they deviate from the reference point. It also proves the latent heat has a direct linear dependence on B, whereas Fig. 3(b) shows the indirect linear dependence of particle size on A, B and E. In addition, particle size has no specific relation with factors C and D.

Optimization

The experimental results were optimized by Design-Expert software using the approximating functions of latent heat and nanoparticle size. To achieve the optimum conditions, all the factors were selected within the studied range while the nanocapsule size and the latent heat set to be minimum and maximum, respectively. The optimization results were listed in Table 4. Then a specific experiment was conducted under optimum conditions to check the accuracy of the results achieved from the model. The experimental and predicted results was presented in Table 5. The results confirmed that the predicted value was in good agreement with the observed value and the model performance was validated. Under the optimal conditions, latent heat is 145.2 J/g representing that 78% of PCM would be encapsulated theoretically according to the following formula [9]:

$$R = \frac{\Delta H^{m}_{NEPCM}}{\Delta H^{m}_{PCM}} \times 100 = 78\% \quad (4)$$

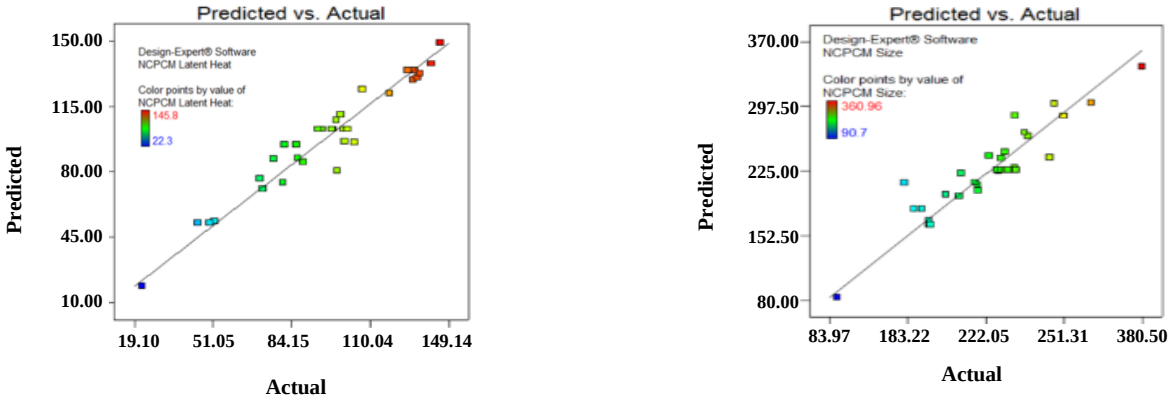

Fig. 1: Predicted vs Actual for for a: Latent Heat 2: Nanocapsules Size models.

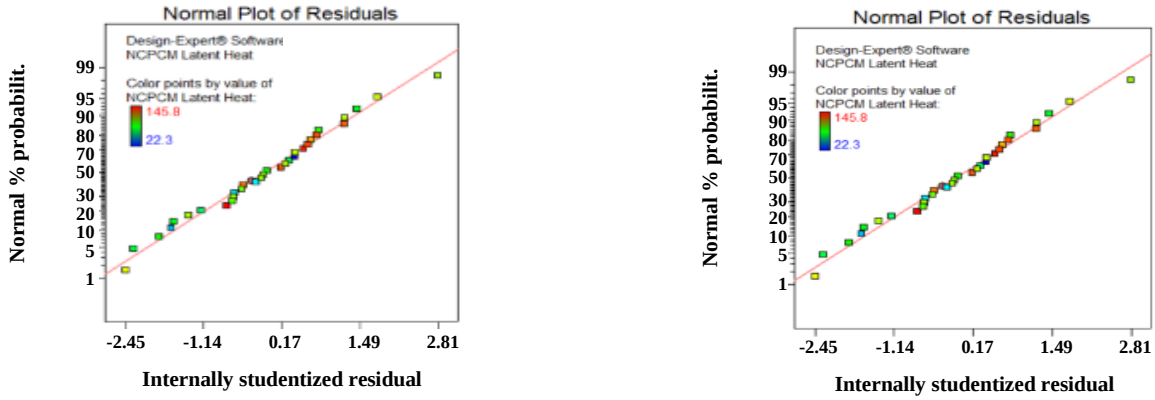

Fig. 2: Normal plot of residuals for a:Latent Heat 2:Nanocapsules Size models.

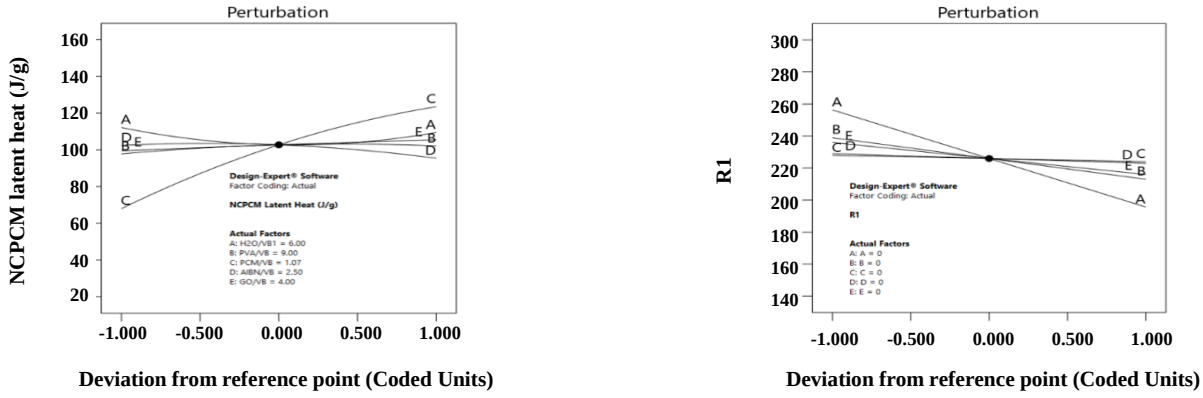

Fig. 3: Perturbation plots for a:Latent Heat 2:Nanocapsules Size models.

Where ΔH^{m}_{NPCM} indicates the melting latent heat of NEPCM, $\Delta H^{m}_{paraffin}$ shows the melting latent heat of PCM, and R is the encapsulation ratio as an indication to the effective performance of a PCM inside the capsule [17].

Nanocapsule characterization

The geometric profiles of the synthesized NEPCMs were investigated using FESEM and TEM techniques. Based on the micrographs (Fig.4), all NEPCMs dispersed well with regular spherical shapes. Some little dimples

Table 4: Optimized values of process variables.

H2O/MMA	wt/wt	11.3
X-100/MMA	wt%	10.81
PCM/MMA	wt/wt	1.88
BPO/MMA	wt%	2.96
GO/MMA	wt%	3.79

Table 5: Experimental and calculated optimal responses.

		Modeling	Experiments
NPCM latent Heat	j/g	145.2	146.8
NPCM Size	nm	156	168±10

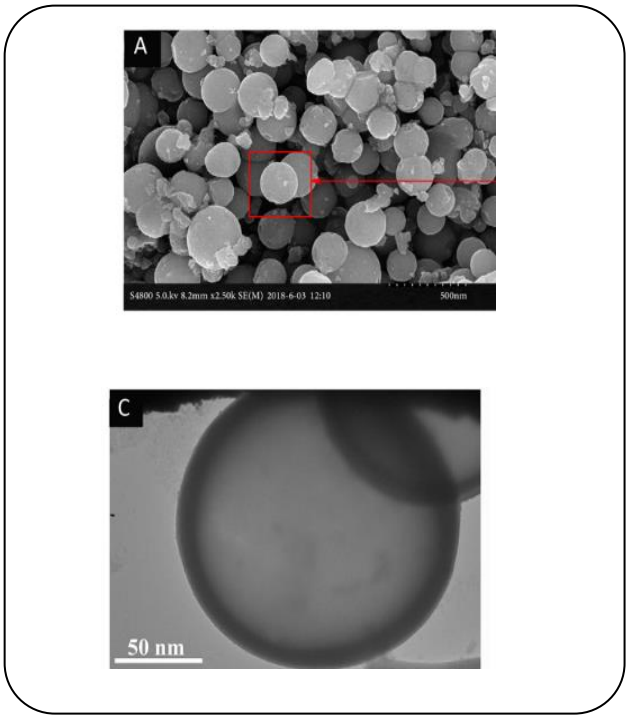

Fig. 4: FESEM and TEM image of nanocapsules.

existed on the NEPCMs surface as a result of producing reserved expansion space during the polymerization process. This may improve thermal stability temperature of NEPCMs. Representative TEM images of NPCM is shown in Fig. 6b. From the TEM image, the NPCM nanosphere exhibited a distinctive core-shell structure with regular spherical shape which is in good agreement with FESEM micrographs. Nanocapsules PSD reveals that the diameter distribution of nanocapsules varied from 60 nm to 330 nm, exhibiting a narrow sized distribution. The average particle size of the nanocapsules was estimated to be about 168±30 nm.

FT-IR spectra of GO, MMA, PCM and NEPCM were illustrated in Fig. 5. Based on the results, some similar chemical structures are found. The peaks observed at 2925 and 2853 cm^{-1} are assigned to stretching vibration of CH_2[21]. In addition, the in-plane bending vibration peaks of CH_2 are located in 1467 and 721cm^{-1}[22]. Additionally, the peak in 721 cm^{-1} is the characteristic peak of $(CH_2)n$ ($n \geq 4$), which belongs to PCM. To sum up, the spectra of NEPCM contain the characteristic peaks of MMA and PCM, which confirms that PCMis encapsulated by MMA. Moreover, no similar peak can be seen between MMA and graphene, indicating that a small amount of graphene has slight effect on the shell structure.

The leakage-prevention is plotted as a function of time and results reported in Fig. 6. According to the data, the PCM leakage rate of NEPCMs significantly decreased when GO incorporated into the shell structure. Since the thickness of GO nanosheets is about 1.2 nm, the GO can be considered to have a monolayer structure. When combined with MMA, the GO nano sheets cooperate with each other closely because of bridging effect via π-π interactions.

Table 6 demonstrated the comparison between the encapsulated PCMs in this study and in the similar recent works:

CONCLUSIONS

Here, a novel type of Graphene Oxide (GO) -modified NEPCM using MMA as the shell material and n-octadecane as the core material was fabricated via mini-emulsion polymerization. Modeling and optimization of nanoencapsulation was were performed using response surface methodology-central composite design (RSM-CCD). H_2O/MMA, X-100/MMA, PCM/MMA, BPO/MMA and GO/MMA mass ratio were the control factors in this study. Two models for melting latent heat and the average size of NEPCM were developed. As a result, H_2O/MMA and X-100/MMA mass ratios showed a positive effect on melting latent heat, while H2O/MMA, X-100/MMA and GO/MMA mass ratios showed a linear negative effect on the average particle size. Process optimization was carried out to maximize the melting latent heat and a maximum melting latent heat of 148.5 J/g was obtained. Compared with nanocapsules without GO,

Table 6: Comparing results with literature.

Sample name	Particle size (μm)	Thermal conductivity (W/mK)	Melting latent heat (kJ/kg)	Reference
PMMA/GO/ n-octadecane	0.1-0.18	0.42	148.5	This study
n-octadecane/SiO_2	7.00–16.00	0.45	123.00	[12]
n-octadecane/SiO_2	17.00	0.31	130.00	[18]
Palmitic acid/AlOOH	0.20	0.84	19.00	[16]
n-eicosane/ZrO_2	1.5–2	–	126.50	[26]

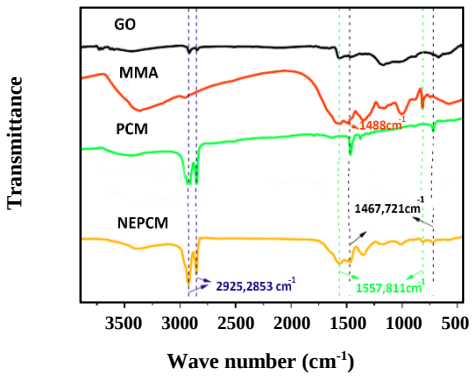

Fig. 5: FTIR spectra of GO, MMA, n-octadecane, NEPCM.

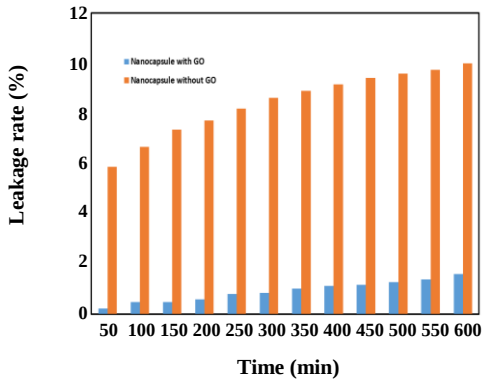

Fig. 6: PCM leakage rate of NEPCMs in release test according to time.

the novel prepared NEPCMs exhibit better leakage prevention and the leakage rate is reduced by about 85% (50 h),. and moreover, the encapsulation ratio is about 78 wt.% which is considerably high rather appreciable.

Received : Sep. 3, 2019 ; Accepted : Dec. 27, 2019

REFERENCES

[1] Alizadeh M., Sadramel S.M., Development of Free Cooling Based Ventilation Technology for Buildings: Thermal Energy Storage (TES) Unit, Performance Enhancement Techniques and Design Considerations – A Review, *Renewable and Sustainable Energy Reviews*, **58**: 619-645 (2016).

[2] Azizi Z., Alamdari A., Doroodmand M.M., Highly Stable Copper/Carbon Dot Nanofluid. Preparation and Characterization, *Journal of Thermal Analysis and Calorimetry*, **133**: 951–960 (2018).

[3] Azizi Z., Alamdari A., Malayeri M.R., Thermal Performance and Friction Factor of a Cylindrical Microchannel Heat Sink Cooled by Cu-Water Nanofluid, *Applied Thermal Engineering*, **99**: 970–978 (2016).

[4] Azizi Z., Alamdari A., Malayeri M.R.. Convective Heat Transfer of Cu–Water Nanofluid in a Cylindrical Microchannel Heat Sink, *Energy Conversion and Management*, **101**: 515–524 (2015).

[5] Chandel S.S., Agarwal T., *Review of Current State of Research on Energy Storage, Toxicity, Health Hazards and Commercialization of Phase Changing Materials, Renewable and Sustainable Energy Reviews*, **67**: 581-596 (2017).

[6] Mohamed S.A., Al-Sulaiman F.A., Ibrahim N.I., Zahir M.H., Al-Ahmed A., Saidur R., Yılbaş B.S., Sahin A.Z., A Review on Current Status and Challenges of Inorganic Phase Change Materials for Thermal Energy Storage Systems, *Renewable and Sustainable Energy Reviews*, **70**: 1072-1089 (2017).

[7] Browne M.C., Norton B., McCormack S.J., Phase Change Materials For Photovoltaic Thermal Management, *Renewable and Sustainable Energy Reviews*, **47**: 762-782 (2015).

[8] Liu C., Rao Z., Zhao J., Huo Y., Li Y., Review on Nanoencapsulated Phase Change Materials: Preparation, Characterization and Heat Transfer Enhancement, *Nano Energy*, **13**: 814-826 (2015).

[9] Graham M., Coca-Clemente J.A., Shchukina E., Shchukin D., Nanoencapsulated Crystallohydrate Mixtures for Advanced Thermal Energy Storage, *Journal of Materials Chemistry A*, **5(26)**: 13683-13691 (2017).

[10] Ling Z., Zhang Z., Shi G., Fang X., Wang L., Gao X., Fang Y., Xu T., Wang S., Liu X., Review on Thermal Management Systems Using Phase Change Materials for Electronic Components, Li-Ion Batteries and Photovoltaic Modules, *Renewable and Sustainable Energy Reviews*, **31**: 427-438 (2014).

[11] Li Y., Yu S., Chen P., Rojas R., Hajian A., Berglund L., Cellulose Nanofibers Enable Paraffin Encapsulation and the Formation of Stable Thermal Regulation Nanocomposites, *Nano Energy*, **34**: 541-548 (2017).

[12] Tahan Latibari S., Mehrali M., Mehrali M., Indra Mahlia T.M., Cornelis Metselaar H.S., Synthesis, Characterization and Thermal Properties of Nanoencapsulated Phase Change Materials *via* Sol-Gel Method, *Energy*, **61**: 664-672 (2013).

[13] Sari A., Alkan C., Döğüşcü D.K., Kizil C., Micro/Nano Encapsulated N-Tetracosane and N-Octadecane Eutectic Mixture with Polystyrene Shell for Low-Temperature Latent Heat Thermal Energy Storage Applications, *Solar Energy*, **115**: 195-203 (2015).

[14] Chen Z.H., Yu F., Zeng X.R., Zhang Z.G., Preparation, Characterization and Thermal Properties of Nanocapsules Containing Phase Change Material N-Dodecanol by Miniemulsion Polymerization with Polymerizable Emulsifier, *Applied Energy*, **91(1)**: 7-12 (2012).

[15] Tumirah K., Hussein M.Z., Zulkarnain Z., Rafeadah R., Nano-Encapsulated Organic Phase Change Material Based on Copolymer Nanocomposites for Thermal Energy Storage, *Energy*, **66**: 881-890 (2014).

[16] Zhang G.H., Bon S.A.F., Zhao C.Y., Synthesis, Characterization and Thermal Properties of Novel Nanoencapsulated Phase Change Materials for Thermal Energy Storage, *Solar Energy*, **86(5)**: 1149-1154 (2012).

[17] Fang Y., Yu H., Wan W., Gao X., Zhang Z., Preparation and Thermal Performance of Polystyrene/N-Tetradecane Composite Nanoencapsulated Cold Energy Storage Phase Change Materials, *Energy Conversion and Management*, **76**: 430-436 (2013).

[18] Tahan Latibari S., Mehrali M., Mehrali M., Afifi A.B.M., Mahlia T.M.I., Akhiani A.R., Metselaar H.S.C., Facile Synthesis and Thermal Performances of Stearic Acid/Titania Core/Shell Nanocapsules by Sol-Gel Method, *Energy*, **85**: 635-644 (2015).

[19] Zhu Y., Liang S., Wang H., Zhang K., Jia X., Tian C., Zhou Y., Wang J., Morphological Control and Thermal Properties of Nanoencapsulated N-Octadecane Phase Change Material with Organosilica Shell Materials, *Energy Conversion and Management*, **119**: 151-162 (2016).

[20] Zhu Y., Liang S., Chen K., Gao X., Chang P., Tian C., Wang J., Huang Y., Preparation and Properties of Nanoencapsulated N-Octadecane Phase Change Material with Organosilica Shell for Thermal Energy Storage, *Energy Conversion and Management*, **105**: 908-917 (2015).

[21] Karthikeyan M., Ramachandran T., *Review of Thermal Energy Storage of Micro and Nanoencapsulated Phase Change Materials, Materials Research Innovations*, **18(7)**: 541-554 (2014).

[22] Sari A., Alkan C., Biçer A., Altuntaş A., Bilgin C., Micro/Nanoencapsulated N-Nonadecane with Poly(Methyl Methacrylate) Shell for Thermal Energy Storage, *Energy Conversion and Management*, **86**: 614-621 (2014).

[23] Torabipoor, O., Azizi, Z., Experimental Study of Convective Heat Transfer Coefficient of MgO Nanofluid in a Cylindrical Microchannel Heat Sink, *Transport Phenomena in Nano and Micro Scales*, **6**: 37-43 (2018).

[24] Heidarshenas A., Azizi Z., Peyghambarzadeh S.M., Sayyahi S., Experimental Investigation of the Particle Size Effect on Heat Transfer Coefficient of Al_2O_3 Nanofluid in a Cylindrical Microchannel Heat Sink, *Journal of Thermal Analysis and Calorimetry*, **141**: 957-967 (2020).

[25] Chananipoor, A., Azizi, Z., Raei, B., Tahmasebi, N., Optimization of the Thermal Performance of Nano-Encapsulated Phase Change Material Slurry in Double Pipe Heat Exchanger: Design of Experiments Using Response Surface Methodology (RSM), *Journal of Building Engineering*, **34**:101929 (2021).

[26] Zhang L., Yang W., Jiang Z., He F., Zhang K., Fan J., Wu J., Graphene Oxide-Modified Microencapsulated Phase Change Materials with High Encapsulation Capacity and Enhanced Leakage-Prevention Performance, *Applied Energy*, **197**: 354-363 (2017).

[27] Dreyer D.R., Park S., Bielawski C.W., Ruoff R.S., The Chemistry of Graphene Oxide, *Chemical Society Reviews*, **39(1)**: 228-240 (2010).

[28] Qi G.Q., Yang J., Bao R.Y., Liu Z.Y., Yang W., Xie B.H., Yang M.B., Enhanced Comprehensive Performance of Polyethylene Glycol Based Phase Change Material with Hybrid Graphene Nanomaterials for Thermal Energy Storage, *Carbon*, **88**: 196-205 (2015).

[29] Yi W., Wu H., Wang H., Du Q., Interconnectivity of Macroporous Hydrogels Prepared via Graphene Oxide-Stabilized Pickering High Internal Phase Emulsions. *Langmuir*, **32(4)**: 982-990 (2016).

[30] Alizadeh M., Sadrameli S.M., Numerical Modeling and Optimization of Thermal Comfort in Building: Central Composite Design and CFD Simulation. *Energy and Buildings*, **164**: 187-202 (2018).